FIBRES & TEXTILES in Eastern Europe

sciendo

FIBRES & TEXTILES in Eastern Europe

Research Article • DOI: 10.2478/ftee-2024-0030 FTEE • 32(4) • 2024 • 31–41

Studies on the Effect of Accelerated Ageing on Structural, Physico-Mechanical and Ballistic Properties of Hybrid Silicone-Ceramics Composites

Katarzyna Kośla[1]*, Edyta Chmal-Fudali[1], Paweł Kubiak[1]

[1] Institute of Security Technologies "MORATEX", Marii Sklodowskiej-Curie 3 Street, Lodz 90-505, Poland
** Corresponding author. E-mail: kkosla@moratex.eu*

Abstract
The aim of this paper was to study and analyze methods of evaluating the service ability and lifespan of ballistic armors made of a hybrid silicone-ceramic (HSC) composites. Experimental tests with accelerated ageing were conducted on the composite ballistic armors in a laboratory to predict and analyze their durability: changes in ballistic performance, as well as physical, and structural properties occurring due to simulated usage conditions. It was proved that despite the changes which took place at the molecular level in the HSC composite materials, accelerated aging processes do not affect the fragmentation resistance level of ballistic HSC inserts.

Keywords
accelerated aging, ballistic silicone-ceramic composites, fragment resistance, infrared spectroscopy, thermogravimetry.

1. Introduction

Bullet-, knife-, and puncture-proof products are the essential elements of soldier protection systems (SPS). These types of protective products, besides the most important factor, which is the ballistic performance, and other threats to the safety level, should also be characterized by certain specific features: ergonomics (especially adjustment to the user's body and air permeability), smooth external surfaces that help the user to wear them under clothing, flexibility, and relatively low weight while maintaining their protection capabilities. Continuous development of various projectile types (specialized materials and newly-developed structures and shapes are used for projectile cores) forces the necessity of increasing the protective effectiveness of SPS without increasing its mass. However, the list of ballistic materials currently used by global armor manufacturers is limited. In addition, it appears that a significant part of these materials, with their configuration in ballistic inserts, had already reached the limit of ballistic protective capabilities, making it extremely difficult to further increase the effectiveness of protection.

One of the basic materials used in ballistic systems is ceramics, which comprises an important group of light armor materials [1-4]. The high strengths of ceramics in combination with their low densities enable the design of weight-efficient armor systems with high protection capability against various fragment and projectile threats. Still, there are many challenges, i.e.:

– A major drawback of ceramics as armor materials is their brittle fracture behavior, which is caused by their inability to accommodate plastic strains. Improving the properties of ceramics in terms of reducing their brittleness is still a challenge and an object of research [3, 5, 6].
– While ballistic ceramics have an important role in breaking up and thus defeating a threatening projectile, proper backing materials for ceramics are mandatory. Such backing layer (aluminum, steel or fibre reinforced plastics (FRP)) adhesively bonded to the ceramic layer must be specifically matched to the design threat and ceramic used in the armor composition [5, 7, 8]. The adhesive must match the ceramic as well as the backing material, but it is prone to ageing.

Typically, FRP's for composite armor consist of multi-layer uni-directional or woven fabrics layers (constituted of high strength low modulus fibres) [9-13]. This design has a high impact energy transfer and a low performance in stopping the projectile, leading to a high number of necessary layers to defeat the threat. To improve the ballistic performance combined with lower weight, novel technologies in terms of materials and ballistic solutions have to be developed.

In recent years, many new solutions based on different hybrid composites and/or ceramic-polymer composite armors have been developed and tested [14-17]. These solutions are particularly interesting for their high strength and energy absorption capability while remaining lightweight. The one of the key functions of ceramics is to retard ballistic impact penetration, and then a polymer panel is to absorb the high energy generated from the propagation of elasticity. One such solution is a flexible, hybrid silicone-ceramic (HSC) composite developed in a previous work [18]. HSC composite consists of five layers of different materials, including:

– outer layers made of elastomer;
– an inner layer made of ceramic tiles placed on a carrier film;
– reinforcement layers made of aramid fabrics and/or foamed polymer materials.

The outer silicone layer acts as a matrix, in which ballistic ceramic tiles are placed,

and allows the composite system to better adjust to the user's body, which increases the ergonomic properties of the armor. Reinforcement layers are intended to limit the additional fragments from the ceramic brittle during the impact of the fragment or bullet on the sample and to contribute to the "stabilization" of the ceramic layer. This phenomenon is understood to limit the process of detachment of adjacent ceramic fragments under the fragment impact [18].

Reinforcement layers can be made of impact-hardening polymers which can significantly improve impact protection because of their particular smart performance material properties, switching between softness and stiffness levels. Several commercial impact-hardening polymers such as Poron®XRD (Rogers Corporation, USA), D3O® (D3O, UK), DeflexionTM (Dow Corning, USA), and Confor® (Trelleborg AB, Sweden), Sorbethane® (Gelmec, UK) are practically applied as impact protective materials [19]. Poron®XRD foams have open-cell structures and density ranging from 240 to 480 kg/m^3, which allows the absorption of sweat produced by the human body. They are also characterized by significant tensile strength (in the range from 482 to 1382 kPa), tearing (in the range from 1.1 to 12.3 kN/m), and a shock absorption capacity in a large operating temperature range from -40°C to 90°C [20, 21]. Shock-absorber D3O® is a closed-cell polyurethane foam composite with polyborondimethylsiloxane as the dilatant dispersed through the foam matrix, which makes the product rate-sensitive, thus dissipating more energy than plain polyurethane at specific energy levels [22]. In contrast, Sorbothane® is shear thinning, solid at rest but becomes more fluid and deformable on impact (i.e., viscosity decreases as the rate of shear increase) [23]. Confor® is a medium-density open-cell polyurethane foam providing a combination of physical properties, energy absorption while maintaining a softening point. Confor® foams are subject to low deformation, very good vibration suppression properties and excellent energy absorption (up to 97%). Having open cells in the structure, they are breathable, which helps to remove moisture and sweat from the body [24]. Deflexion® is a silicone material which disperses and absorbs the high impact energy, e.g. from a bullet shot, thus it can be used in bulletproof vests [19].

The ballistic properties and ability to absorb a high-energy impact resulting from the impact of a bullet or fragment in the HSC composite depend on the properties of the ceramic elements. However, if users wear this type of composite, the time and effectiveness of protection will depend mainly on the resistance of the external and reinforcing layers to accelerated aging processes. Especially, the impact of aging processes on material parameters such as: the tensile and/or tear strength of silicone and PU and the adhesion strength of the self-adhesive film with ceramic elements [18].

Ageing (i.e. the change of material properties over time caused by external parameters like temperature, humidity, UV radiation, etc.) is a very complex topic due to the sheer number of parameters which could affect different properties of a material [25-28]. While today these effects have been studied on different materials in use in protective equipment (especially in polymers), there is still no comprehensive study which links these effects to changes in the protective performance. Therefore, these effects cannot be measured or predicted reliably, which might either cause ballistic systems to be replaced prematurely. leading to high operating costs, or be related to the potential risk of injury or death to users. Changes in the physico-mechanical properties can be a strong drawback in maintaining the protection of the armor. The reasons for these physico-mechanical property changes can be in the microstructure or chemical structure, from chemical reactions or water absorption by the materials [29-32]. These phenomena might be induced by long time exposure to raised temperatures, the presence of moisture or UV radiation. For instance, the energy brought by temperature or radiation can activate some degradation or chemical reaction processes. Similarly, water absorption can induce hydrolysis reactions inside some polymers, leading to the presence of faults or structural damage.

Therefore, studies of the accelerated aging of previously developed new hybrid silicone-ceramic composites are the subject of this publication.

2. Materials and Methods

2.1. Materials and samples tested

To produce the hybrid silicone-ceramic (HSC) composites, the materials listed below were used:

- hexagonal ceramics tiles made from aluminum oxide (Al_2O_3 content 98%, CeramTec, Plochingen, Germany) with a tile thickness equal to 3.0±0.2 mm,
- Za 22 Mould (Zhermack, Badia Polesine, Italy) silicone elastomer – marked as silicone,
- Poron® XRDMA(Polting Foam Sp. zo.o, Gliwice, Poland) with thickness 3.0±0.2 mm and areal density 555±12 g/m^2 –marked as PU foam,
- Twaron® CT612 (Teijin, Wuppertal, Germany) with areal density 123±1 g/m^2,
- self-adhesive film 4622/WS 40 (Bochemia, Radom, Poland) forming a carrier film on which ceramic elements were placed. The film is made of a polyester mesh with a diameter of 1.5 mm, coated with synthetic resins with a grammage of 155±5 g/m^2.

Method of preparing hybrid silicone-ceramic composites was presented in detail in a previous work [18].

Accelerated ageing studies were performed for:

1. HSC composites used in combination with a soft ballistic insert with a surface mass of 5.5±0.5 kg/m^2, consisting of sheets of Twaron® CT612 p-aramid fabric,
2. samples of raw materials Za 22 Mould (silicone) and Poron® XRDMA (PU foam), as well as self-adhesive film 4622/WS 40 (self-adhesive film) used

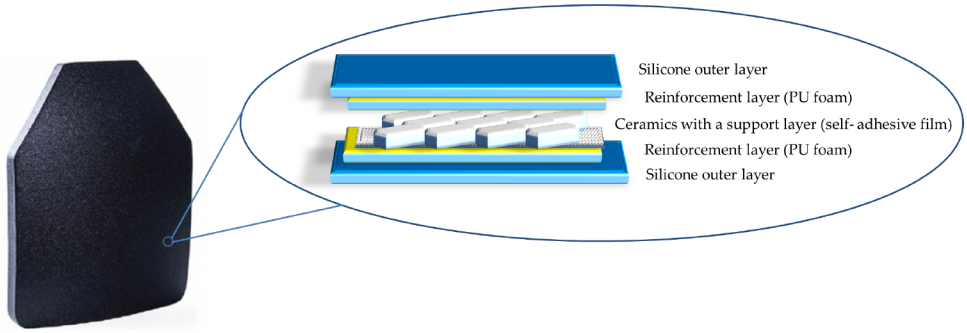

Fig. 1. Scheme with the composition of the HSC composite

in the construction of hybrid silicone-ceramic (HSC) composites with sizes defined in relevant standards and/or test procedures.

The results of the aging tests for the Twaron® CT612 material are presented in article [28].

2.2. Accelerated aging process

The accelerated aging process was performed by incubating the samples in a KMF 240 thermostatic chamber (BINDER GmbH, Germany) at a set temperature of (60±2)°C and humidity of (50±2)% over a time interval of: 63, 129 and 194 days, which equals the time of use of inserts in real conditions of 2, 4, and 6 years, respectively.

The simulation of the accelerated aging process was performed using the Arrhenius formula (1), according to ASTM 1980F - 2021 ed. "Standard Guide for Accelerated Aging of Sterile Barrier Systems for Medical Devices":

$$AAF=Q_{10}^{[TAA-TRT/10]}, \quad (1)$$

where: AAF – accelerated aging factor; TAA – accelerated aging temperature [°C]; TRT – storage temperature in the real-time aging of the sample [°C], Q_{10} – aging factor, determined using the kinetics of changes in the selected property/parameter of the material, for temperature changes of 10°C.

The following equation was used to calculate the actual aging time:

$$ATT=(365 \text{ days})/AAF, \quad (2)$$

where: ATT – the time of accelerated aging, which is equivalent to the real-time aging (corresponding to 2, 4 or 6 years of use under real conditions). AAF – accelerated aging factor;

The Q_{10} aging factor, which defines the aging function curve, was set at the level of 2, and the value of the TRT parameter was set at 25°C. In turn, the accelerated aging temperature TAA was set at (60±2)°C. According to the guidelines, its value should be within in the range from 50°C to 60°C, which is related to the fact that higher temperature significantly reduces the process time, however, it may adversely affect the structural properties of the tested materials, and consequently, the tested materials may show results different from normal.

2.3. Fatigue tests simulating mechanical loads of HSC composites

The fatigue tests simulating the mechanical loads of HSC composites involved bending both ends of the samples in an S 625 device, produced by PPU STOGUM (Poland), according to parameters determined on the basis of the following formula [28, 33]:

$$N=n\times x\times k, \quad (3)$$

where: N – the number of deformation cycles on the S 625 device; n – the number of days of effective insert exploitation per year (values of n were assumed to be equal to 52, 156 or 260); x – simulated time of use (values from 2 to 6 years were assumed); k – the number of daily deformations (the value of 30 was taken for investigations).

Therefore, the research defined the number of deformation cycles as:
- 9360 cycles, which corresponds to the estimated use of the insert once a week over 6 years;
- 18 720 cycles, which corresponds to the estimated use of the insert twice a week over 6 years;
- 28 080 cycles, which corresponds to the estimated use of the insert three times a week over 6 years;

The research also assumed a testing angle equal to 30° and a duration of a single cycle of 4 s.

2.4. Physico-mechanical properties tests

The physical and mechanical parameters of silicone elastomer and PU foam, such as: density, hardness, and tensile strength were tested according to the methodology described below.

2.4.1. Density

The density was calculated from the following formula:

$$\rho=(A/A-B)\times \rho_0 \quad (4)$$

where: ρ – sample density (g/cm^3), A – weight of sample in air (g), B – weight of sample in liquid (g), ρ_0 – density of liquid (g/cm^3).

2.4.2. Hardness

Silicone elastomers were characterized in terms of their hardness. Hardness measurements were carried out in accordance with PN-EN ISO 868:2005 using a Shore A hardness tester mounted on a tripod. The hardness result was read after 15 seconds. Five hardness measurements were made for each sample, and the average of the five measurements was given as the result.

2.4.3. Tensile tests

Determination of mechanical properties of silicone elastomer at static tension was performed in accordance with PN-ISO-37:2007. A tensile test was carried out on standard paddle or ring shaped samples in a testing machine (Instron) at a constant tensile speed. The tensile stress was calculated as the force in relation to the unit of area of the initial cross-sectional area of the measuring section of the tested elastomer sample. Tensile strength is defined as the maximum recorded tensile stress and the elongation at break as the deformation of the measuring section at break. In such a method of determining the tensile strength of elastomers, the effect of transverse deformation of the sample during the test is not taken into account.

The values of the maximum tensile force for PU foam were determined using ISO 1798:2008 "Flexible cellular polymeric materials — Determination of tensile strength and elongation at break". The maximum stretching force and relative elongation at maximum force for self-adhesive film were determined in accordance with PN-EN ISO 13934-1:2013-07 "Textiles. Tensile properties of fabrics. Part 1: Determination of maximum force and elongation at maximum force using the strip method". Adhesion strength were determined using PN-EN ISO 2411:2017-11 "Rubber- or plastics-coated fabrics. Determination of coating adhesion".

Each of the tested physico-mechanical parameters was determined for at least 5 samples and the values obtained averaged. The error values reported are the expanded uncertainty with a coverage factor of k=2 and an assumed confidence level of 95%.

2.5. Analysis of thermal properties using thermogravimetry (TG)

Thermal analyses were performed using a TGA/DSC3+ thermogravimetric analyzer (Mettler Toledo, Switzerland). The measurement was carried out in an inert gas (nitrogen) atmosphere using an alumina crucible with a capacity of 70 µl. The analysis was performed using the following measurement program: heating 25°C to 900°C, heating rate 5°C/minute and/or 10°C/minute. The measurement results are presented in the form of thermograms.

2.6. Structural testing using infrared spectroscopy (FT-IR)

FT-IR analysis was performed on both samples for accelerated aging and not, using a NICOLET iS10 spectrophotometer (Thermo Scientific, USA) within the wavelength range from 400 to 4000 cm^{-1}. Measurements were carried out using a DTGS KBr detector, with a resolution of 4. For FTIR-ATR testing, the material was cut to dimensions of 20×20 mm and applied to the crystal by pushing it down in a suitable manner. Both the background spectrum (i.e., the spectrum of the crystal) and the spectrum of the crystal with the sample were measured. The background measurement was saved in the internal memory of the spectrophotometer and automatically subtracted from the sample measurement as a correction for the external conditions of the tests. The FT-IR analysis was repeated 3 times for each sample; if the standard deviation was within 5%, no further repetition of the study was performed.

2.7. Surface morphology studies performed by scanning electron microscopy (SEM)

Measurements were made using an HR-SEM high-resolution electron microscope (High resolution FEI Nova Nano SEM 450 electron microscope with EDS, Thermo Fisher Scientific Inc., USA) with the use of a highly sensitive CBS (Circular Backscatter) detector with 4 concentrically arranged sectors, enabling the detection of backscattered electrons (BSE) and cooperating with the electron energy deceleration mode. The measurements were carried out at accelerating voltage values of 3 and 5 kV and under magnifications of 500× and 1500×.

2.8. Fragment resistance measurements

The samples intended for the assessment of fragment resistance were HSC composites, consisting of Al2O3 ceramics, Poron® XRDMA and Twaron®CT612 embedded in Za Mould 22 elastomer, used in combination with a soft ballistic insert with a surface mass of 5.5±0.5 kg/m^2, consisting of sheets of Twaron® CT612 p-aramid fabric.

The resistance to fragments was determined on the basis of the ballistic limited velocity parameter (V50). V50 was measured at ambient temperature according to STANAG 2920 "Ballistic test method for personal armor materials and combat clothing". The limit of ballistic protection V50 was determined as the average of the equal number of the highest measured speeds of the fragment causing only partial puncture and the lowest measured speeds causing total puncture within the velocity spread $\Delta \leq$ 40 m/s. An FSP.22 standard fragment with a mass of (1.10÷0.03) g, diameter of (5.38±0.02) mm and length of 6.35 mm, made of steel with a hardness of (30±2) HRC was used for the fragment resistance tests.

3. Results

3.1. Results of structural and thermal tests of materials used in the construction of HSC composites

In the first part of this work, FT-IR structural studies were carried out to determine possible changes at the molecular level after accelerated aging processes in the silicone structure and PU foams. The FT-IR spectra obtained were summarized and presented in Figure 2.

The spectrums obtained for silicone (Fig. 2a) are characterized by the occurrence of bands at wavelengths of 660–690 cm^{-1}, corresponding to the bending oscillation of single carbon bonds. The presence of a low intensity band in the wavelength range 761 cm^{-1} corresponding to bending vibrations of C–H bonds was also observed. Moreover, the presence of bands at wavelengths of 801 cm^{-1} and 865 cm^{-1} was observed from the deformed pendulous oscillation of the CH_3–Si–CH_3 group, and 1021 cm^{-1} and 1093–1094 cm^{-1} - characteristic for the asymmetric tensile oscillation of the Si–O–Si group. Based on the analysis of the FT-IR spectrums obtained, the presence of bands characteristic for symmetrical and asymmetrical deformation oscillations of Si–CH_3 groups can also be noted, with wavelengths of 1261 cm^{-1} and 1411 cm^{-1}, respectively. The bands in the range of wave numbers 2905 cm^{-1} and 2963 cm^{-1} characteristic for the tensile oscillations of C–H bonds, indicate the presence of methyl groups in the silicone molecule. However, no bands in the range of 2160–2170 cm^{-1} were recorded, which indicates the absence of –SiH groups in molecules of the compounds used. The FT-IR spectra also indicate that after a period of accelerated aging simulating a 6-year period of silicone use, there is a decrease in the intensity of the bands coming from the vibrations of the CH_3–Si–CH_3, Si–CH_3 groups in the wavenumber range of 801 and 1261 cm^{-1} and in the intensity of the band located at a wave number of 1094 cm^{-1} originating from the vibration of Si–O–Si bonds, which may result from the breaking of Si–C and Si–O bonds and the formation of trace amounts of cyclic oligomers [34, 35].

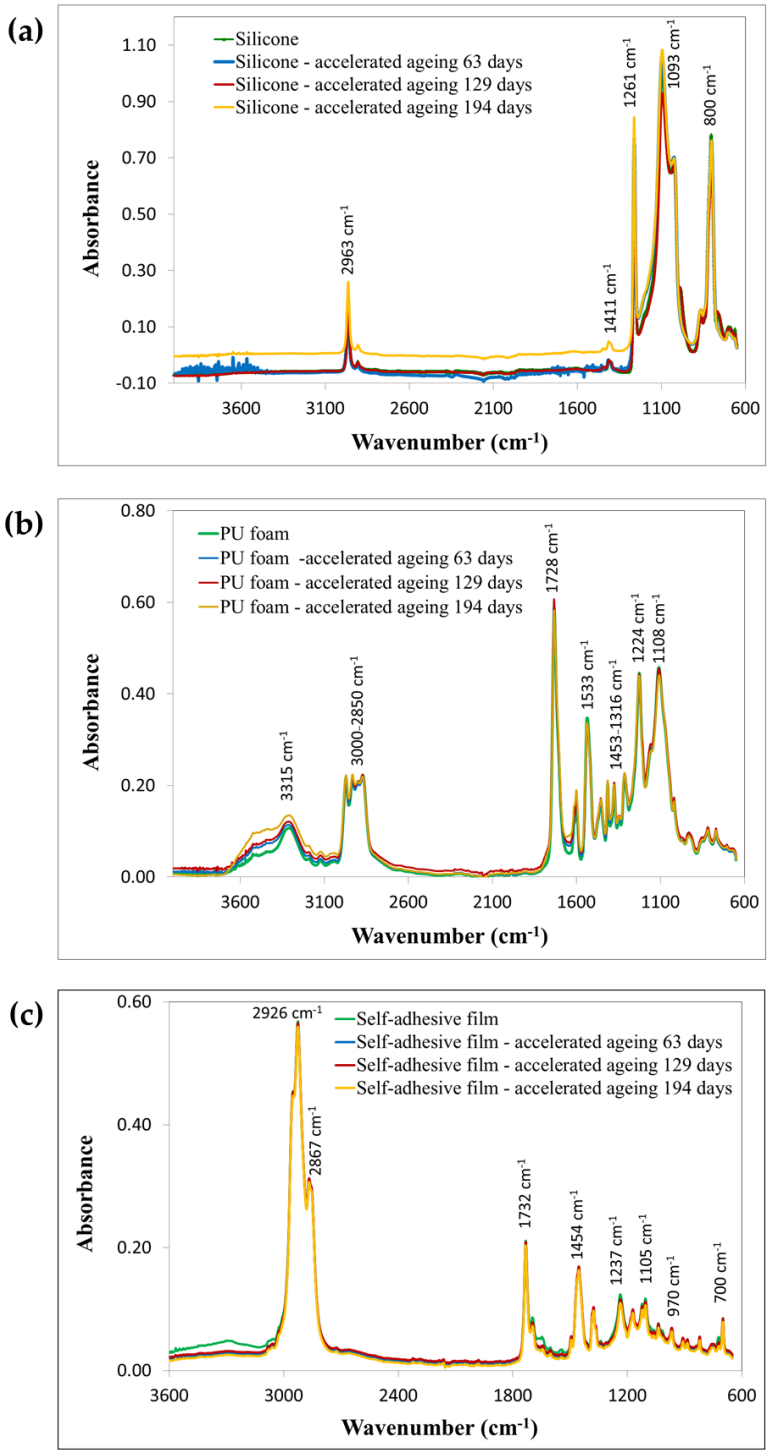

Fig. 2. FT-IR spectra: a) silicone, b) PU foam, c) self-adhesive film, before and after accelerated ageing process

In the PU foam sample (Fig. 2b), the following characteristic absorption bands were found: 3315 cm^{-1} - attributed to the stretching vibration of N–H bonds that form intermolecular hydrogen bonding, 3000–2850 cm^{-1}, indicating the asymmetric and symmetrical stretching vibrations of the methyl groups. The band located at the wavenumber value of 1533 cm^{-1} corresponds to the N–H deformation, and the bands present at the

wavelengths in the range 1728–1602 cm^{-1} are attributed to the stretching vibration of C=O bonds. The absorption band at 1224 cm^{-1} is attributed to the asymmetric stretching vibration of C−O−C bonds of ester groups. The bands located in the range of 1453-1316 cm^{-1} correspond to deformation vibrations of the $–CH_2–$, $–CH_3$ and/or C–N bands, and the band with the wavenumber value equal to 1108 cm^{-1} corresponds to the vibration stretching of C–N or C–O bonds or vibrations of the Si–O–Si group derived from possible additive/fillers contained in the PU foam [19].The results above indicate that polyurethane is the main component of the foam. For PU foam samples subjected to accelerated aging corresponding to a period of 6 years of use, the following were found: an increase in the intensity of the bands located at wavelengths of 3315 cm^{-1} and 1602 cm^{-1} , corresponding to the stretching vibrations of the N–H groups and the vibrations of the carbonyl group, respectively; a decrease in the intensity of the 1728 cm^{-1} band, corresponding to the stretching vibrations of the C=O bonds, and in the 1533 cm^{-1} band, which corresponds to the N−H deformation. In addition, the intensity of the band assigned to the vibrations of the C–N/C–O and/or Si–O–Si group was reduced (1108 cm^{-1}). The reduction in the intensity of the above-mentioned bands indicates a slow degradation of the urethane bond under the influence of environmental factors affecting the polyurethane as part of the accelerated aging process.

For the self-adhesive film (Fig. 2c), the following bands were noted: 2968 cm^{-1}, 1732 cm^{-1}, 1718 cm^{-1}, 1505 cm^{-1}, 1471 cm^{-1}, 1409 cm^{-1}, 1237 cm^{-1}, 1120-1105 cm^{-1}, 1020 cm^{-1}, 970 cm^{-1}, 794 cm^{-1}, assigned to vibrations of –C–H bonds of methylene and methyl groups and C=O, –C–O– bonds of ester groups coming from the polyester of which the mesh is composed. In addition, the studies showed the presence of bands located in the wavenumber range 2926–2867 cm^{-1}, 1454 cm^{-1}, 1401 cm^{-1} or 700 cm^{-1}, which indicate the presence of an adhesive layer, probably based on polyterpenes. The accelerated aging process caused a slight decrease in the intensity of all spectral bands, especially the bands located at wavenumber values of 1732 cm^{-1} and 1718 cm^{-1} and for the range of 1237-1020 cm^{-1}, as a result of changes in the structure of polyester mesh fibers. The intensity of the 2926 cm^{-1} band originating from the vibrations stretching the C–H bonds of the methylene group present in the adhesive resin also decreased, indicating structural changes in the self-adhesive film.

In order to determine whether the FT-IR results obtained are statistically significant, an ANOVA statistical analysis in accordance with Tukey HSD/ Tukey Kramer for silicone, PU foam and self-adhesive film samples before and after accelerated ageing was performed. The significance level **(a)** was assumed as **0.05**. For p-values $<\alpha$, H_0 is rejected, and the difference between the sample averages of some groups is enough to be statistically significant. This means the ageing process statistically affects structural properties of specified materials used in HSC composite.

The physico-mechanical properties of impact protection materials strongly depend on the internal cellular structures of these materials, such as cell type, cell fraction, cell size and size distribution, etc. Therefore, the surfaces and internal cellular structures of PU foam and silicone were studied using an SEM microscope. The results obtained are presented in Figure 3.

Images taken using SEM microscopy, presenting the morphology of silicone, did not show any structural changes after the accelerated aging process. In both cases (before and after accelerated aging processes), the silicone samples were characterized by the presence of a significant number of globules with sizes ranging from several dozen nanometers to approximately 7 μm.

SEM images of the PU foam surface indicate that the polymer material used in its construction has a porous structure with open pores with a diameter of 40 to 100 μm. Comparison of images obtained for the material surface before and after the accelerated aging processes did not reveal any significant changes in the surface structure of the material.

The HSC composite materials were also analyzed thermogravimetrically in a nitrogen atmosphere, in the temperature range from 25 to 900°C, in order to assess the impact of their chemical structure on thermal stability. Figure 4 shows thermograms of the initial samples and those subjected to accelerated aging processes, simulating use in real conditions, for up to 6 years. Additionally, Table 1 presents the numerical values of the thermogravimetric analysis of the tested materials.

The results of thermogravimetric (TG) analysis (Fig. 4a) indicate a relatively high thermal resistance of the silicone obtained compared with different types available on the market that can be used in composites, especially high temperature vulcanizing (HTV) silicones. The thermogram is characteristic of siloxanes. The TG curve obtained for silicone shows two stages of decomposition: the first one in the temperature range of 103-410°C, in which the mass loss is up to 10%, and the second one in the temperature range of 410-785°C (mass loss of 40%). The value of the T5 parameter (the temperature at which 5% mass loss occurred) increases with an increase in the length of accelerated aging cycles. This increase is approximately 8% for the accelerated aged silicone, reflecting 6 years of use, and is likely related to the structural changes in the silicone described above, based on the analysis of the FT-IR spectra.

In the case of both unaged silicone and silicone subjected to accelerated aging processes, the thermograms did not show a characteristic, small increase in the sample mass in relation to the formation of new Si–O–Si bonds and the oxidation of Si–H bonds, which most often takes place after the first stage of decomposition of the tested materials. It is related to with two aspects, firstly, the lack of Si–H groups in the structure of silicone elastomers, which is confirmed by FT-IR spectra (Fig. 2a).This is also due to the breaking of Si–O–Si bonds and the simultaneous loss of mass

No.	Tested sample	Parameter	Before ageing	Accelerated ageing 63 days	Accelerated ageing 129 days	Accelerated ageing 194 days
1	Silicone	T5 [°C]	272±8	274±9	282±8	293±9
3	PU foam	T5 [°C]	262±7	266±8	268±7	265±7
4		T50 [°C]	334±9	337±8	355±10	355±9
5	Adhesive film	T5 [°C]	221±6	220±8	221±7	222±8
6		T50 [°C]	414±12	413±11	412±11	414±10

Table 1. 5% and 50% temperature-induced mass loss of samples of materials forming the HSC composite

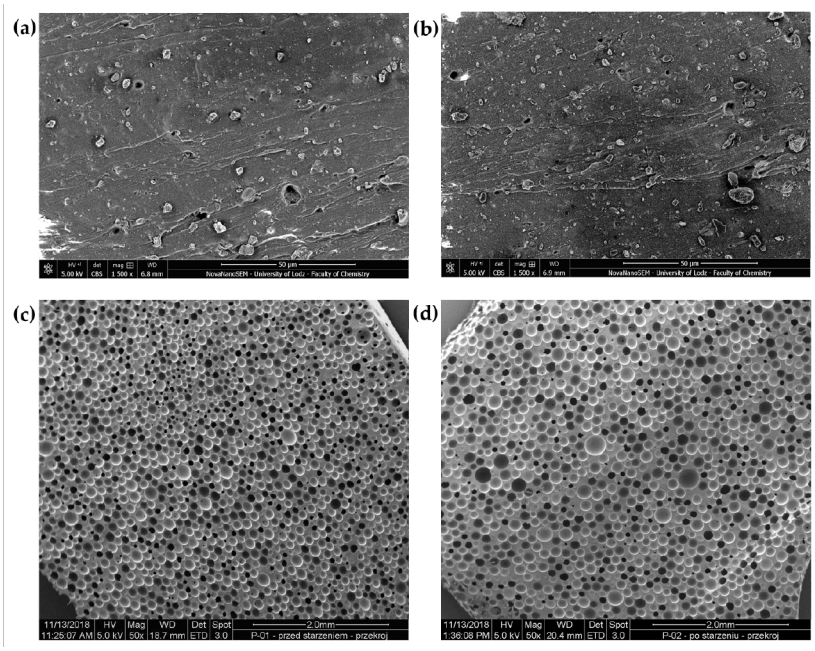

Fig. 3. SEM images obtained for a) non-aged silicone, b) silicone after accelerated aging processes, c) non-aged PU foam, d) PU foam after accelerated aging processes

resulting from the degradation of methyl groups present in the structure of the tested material. The results of thermogravimetric tests obtained are consistent with the literature data obtained for other polydimethyl-siloxanes, i.e. Sylgard 184 (Dow Corning) [34].

Thermogravimetric analysis of the PU foam (Fig. 4b) indicates that thermal degradation under a nitrogen atmosphere is consistent with that of polyurethane, and very possibly polyurethane/SiO_2 composite [36-38]. PU foam shows a multiple-step decomposition. The temperature value at which there is a 5% loss in the mass of PU foam does not change significantly after accelerated aging processes (differences within the range of 6°C, i.e. approximately 2% for the unaged and aged samples). However, in the case of a temperature value for 50% mass loss (T50), thermogravimetric data indicate a slight increase in the value of the T50 parameter with an increase in the number of accelerated aging cycles (a difference of approximately 20°C, which is a change of over 6%).

In the case of thermogravimetric tests of the adhesive film (Fig. 4c), there were no changes in the values of the T5 and T50 parameters as a result of accelerated aging processes, so it should be assumed that this film does not significantly change its thermal properties as a result of aging processes. Thermogravimetric curves indicated the presence of a two-stage decomposition process of the self-adhesive film under the influence of temperature, which is consistent with the composition of the film. The first stage involves the decomposition of glue based on synthetic resins, while in the second stage, the polyester mesh decomposes. In the case of polyester mesh, the mass loss in the samples is due to thermal decomposition into CO and carbonaceous char.

3.2. Results of physico-mechanical properties of materials used in the construction of the HSC composite

Research was also carried out to assess the physico-mechanical properties of materials used in the construction of the HSC composite. The results of physical and mechanical tests for the initial samples and those subjected to accelerated aging processes are presented in Table 2.

The density and hardness values obtained for silicone and PU foam practically do not change for the initial samples and samples subjected to accelerated aging processes. Minor deviations are within the limits of measurement errors. Also, in the case of tensile strength, no significant changes in this parameter were observed for PU foam and silicone samples subjected to accelerated aging compared to unaged samples. In the case of silicone, an increase in tensile strength of approximately 14% was observed, and in the case of PU foam, a decrease in the value of this parameter of approximately 9% after accelerated aging cycles corresponding to a 6-year period of use. These data indicate that structural changes occurring as a result of aging processes only slightly affect the tensile strength of silicone and PU foam.

An increase in the values for the parameters of self-adhesive film such as:

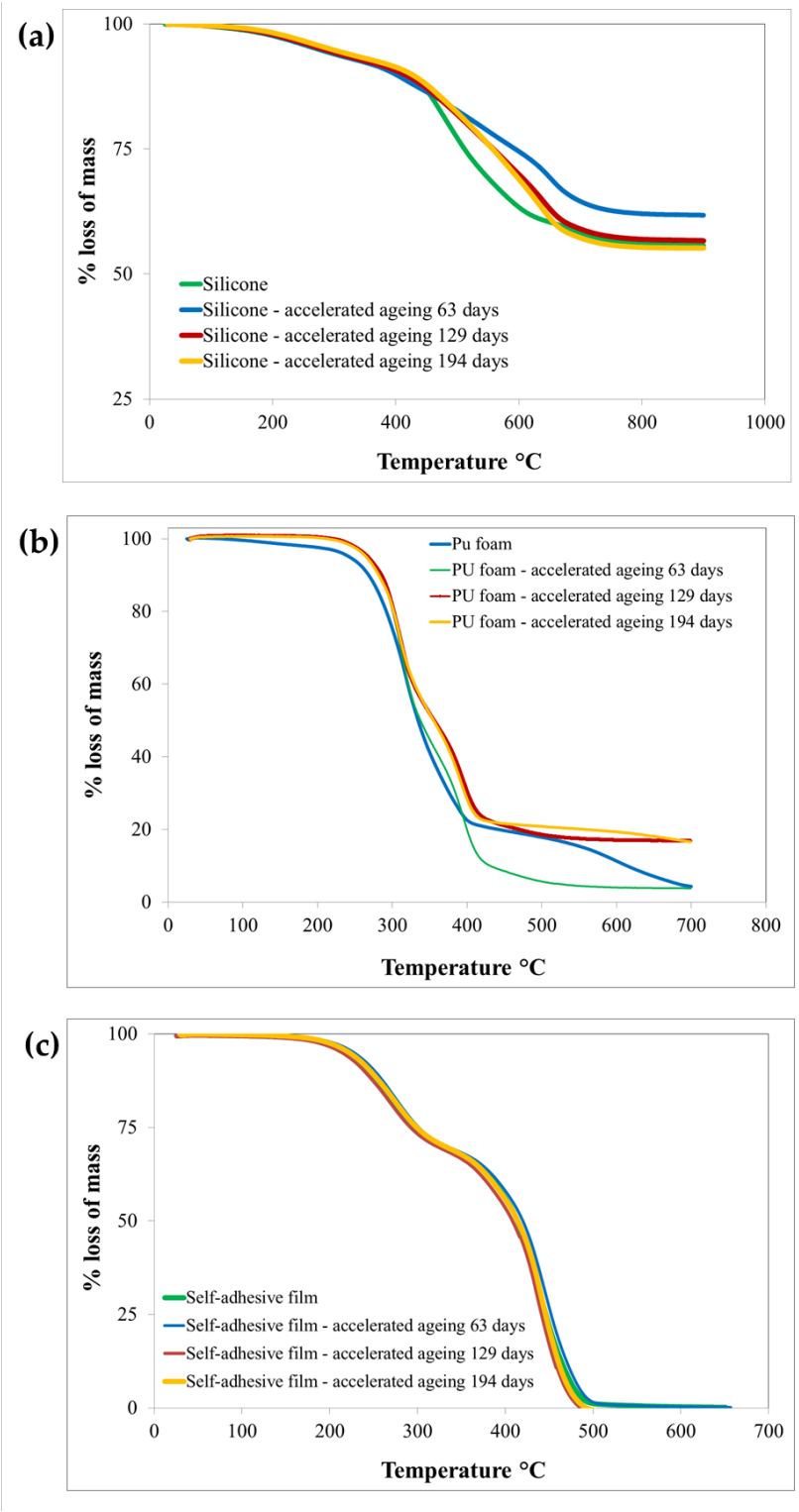

Fig. 4. Thermogravimetric curves showing the mass changes of silicone sample (a), PU foam sample (b) and self-adhesive film sample (c) – unaged and subjected to accelerated aging processes – with increasing temperature

the maximum stretching force, relative elongation at maximum force and the adhesion force was obtained for samples subjected to accelerated aging processes as compared to unaged samples. In the case of self-adhesive film subjected to a period of 194 days of accelerated aging corresponding to 6 years of usage in real conditions, an increase in the maximum stretching force of 19%, an increase in the relative elongation at a maximum force of 36% and an increase in the adhesion force of 59% were achieved as compared to the samples not subjected to accelerated aging processes.

The improvement in the physical and mechanical parameters and in the strength of the connection is the result of the continuation of the adhesive hardening processes, which strengthen the adhesive connections [39].

Adhesive joints usually undergo thermal degradation processes under the influence of increased thermal energy, which causes a decrease in strength [40]. The reason for the loss of strength is the deterioration of both the cohesive parameters of the adhesive film and the adhesive parameters on the phase contact surface. Adhesive subjected to long-term exposure to increased thermal energy oxidizes and thermally decomposes. This increases its brittleness and thus reduces its cohesive strength. On the other hand, at the phase boundary, as a result of adhesive shrinkage, shrinkage stresses and chemical reactions occur on the glued surface [39, 41]. However, due to the fact that the nature of aging depends on the type of glue, joined materials and environmental conditions, the changes in the strength of the adhesive joint during aging does not always have to be negative from the beginning of exposure to environmental factors affecting the adhesive, which was probably the case with the research results presented in this publication.

3.3. Results of fragment resistance tests of HSC composites

The samples intended to assess resistance to fragments were HSC composites combined with "soft" ballistic inserts sewn into the cover. The samples were tested to determine the fragment resistance parameter (V50 parameter) after:

– cycles of accelerated aging simulating the usage life of ballistic composites ranging from 2 to 6 years;
– fatigue tests simulating periods of use from 1× to 3× per week for 6 years.

No.	Sample	Parameter	Methodology	Initial	Accelerated ageing 63 days	Accelerated ageing 129 days	Accelerated ageing 194 days
1	Silicone	Density [g/cm^3]	PBCH-09/2017	1.09±0.04	1.11±0.01	1.12±0.01	1.10±0.02
2		Hardness [ShA]	PN-EN ISO 868:2005	21.0±1.0	21.0±1.0	21.0±1.0	23.0±1.0
3		Tensile strength [MPa]	PN-ISO 37:2007/ AC1:2008	2.1±0.1	2.2±0.1	2.2±0.1	2.4±0.3
4	PU foam	Density [g/cm^3]	PBCH-09/2017	0.17±0.03	0.19±0.02	0.18±0.01	0.19±0.02
5		Hardness [ShA]	PN-EN ISO 868:2005	2.0±0.5	2.0±0.5	2.0±0.5	1.8±0.4
6		Tensile strength [MPa]	ISO 1798:2001	446±29	436±27	419±32	407±31
7	Self-adhesive film	Max. stretching force [N]	PN-EN ISO 13934-1:2013-07	123±3	131±3	140±3	146±3
8		Relative elongation at max. force [%]	PN-EN ISO 13934-1:2013-07	15.0±0.5	17.3±0.5	18.9±0.5	20.4±0.5
9		Adhesion strength [N/50 mm]	PN-EN ISO 2411:2017-11	1.14±0.13	1.37±0.23	1.62±0.31	1.81±0.35

Table 2. Results of physico-mechanical tests

No.	Tested sample	Average value of V50 [m/s]	D [m/s]
1	HSC initial	1240	36
2	HSC aged by 63 days	1221	38
3	HSC aged by 129 days	1235	37
4	HSC aged by 194 days	1246	35
5	HSC fatigue test 9 360 cycles	1250	37
6	HSC fatigue test 18 720 cycles	1253	39
7	HSC fatigue test 28 080 cycles	1259	37

Table 3. Resistance to fragmentation of HSC composites before and after accelerated aging processes and after fatigue tests

The test results (Table 3) were summarized and compared with the data obtained for HSC composites not subjected to accelerated aging cycles.

The HSC composite does not show any significant changes in its fragment resistant properties under the influence of accelerated aging processes corresponding to a period of 2, 4 or 6 years of use, and as a result of fatigue tests which correspond to a period of use of up to 3 times a week over 6 years.

In order to determine whether the resistance to fragmentation results obtained are statistically significant an ANOVA statistical analysis was performed in accordance with Tukey HSD/Tukey Kramer for initial HSC composites, and HSC after accelerated ageing cycles and after fatigue tests. The significance level **(a)** was assumed as **0.05**. For HSC composite p-values >α, the averages of all groups were assumed to be equal. This means the ageing and fatigue processes statistically do not affect fragment resistant properties of the HSC composite.

The value of the V50 parameter of resistance to fragmentation was not determined for the use of the developed HSC composite for periods with a higher frequency than a use of >3× per week during 6 years, because the outer silicone layer began to show signs of degradation consisting in the appearance of kinks and creases on the silicone surface. Therefore, it should be considered that a frequency of use of 3 times a week for a period of 6 years is the limit frequency ensuring the stability of ballistic protection parameters and the safety of potential users of the ballistic composite.

The research showed that the ballistic resistance of the HSC composite is the result of the destruction of ceramic elements by the fragment and the pulling, rupture, decrumbing and extension of yarns and fibers occurring in the soft ballistic insert. The outer silicone layer makes a slight contribution to the fragments' stopping mechanism [18]. It acts as a matrix in which ceramic elements are placed and allows the composite system to adjust to the user's body, which increases the ergonomic properties of the armor. The research conducted allowed to determine that reinforced layers (PU foam) and self-adhesive film also do not affect the fragment-resistant properties of the HSC composite. They are intended for the "stabilization" of the ceramic layer and limit the generation of secondary fragments from the ceramic fragments formed during the impact of a fragment or bullet on the sample [18].

4. Conclusions

Based on the test results obtained, it was proved that accelerated aging processes affect the structural properties of the materials from which the HSC composite

was made, which was confirmed using FT-IR spectra. Structural changes occurring at the molecular level for silicone and PU foam have a small impact on the thermal properties (changes in the values of the T5 and T50 parameters in thermogravimetric tests) and, at the same time, do not cause significant changes in the physico-mechanical properties of these materials. In the case of self-adhesive film, changes in the structure of adhesive and mesh molecules caused by accelerated aging processes contributed to changes in physico-mechanical parameters such as the maximum stretching force, relative elongation at the maximum force and the adhesion force.

In summary, accelerated aging processes cause minor changes at the molecular level in the individual materials from which the HSC composite was manufactured. However, they do not effect significant changes in macroscopic terms nor in the ballistic properties of the composite, such as fragment resistance. Ballistic properties of the HSC composite proposed depend mainly on physico-mechanical parameters, such as hardness, resistance to brittle cracking and Young's modulus of ceramic elements, and such parameters were proved to be constant in the assumed ageing time.

The results of the tests obtained in the paper prove that the HSC composite developed can be used in the construction of ballistic inserts used in applications related to personal protective equipment, i.e. bullet- and fragment-resistant vests. Moreover, the HSC composite developed may be an alternative to the currently used ballistic composites produced in the thermal-pressure pressing process based on aramid or UHMWPE materials, as well as steel or titanium alloy ballistic armor.

Funding

This research was funded by the National Centre for Research and Development, Poland, under project No. POIR.04.01.04-00-0007/18-00, implemented as part of the Smart Growth Operational Programme 2014–2020 (supported by the European Regional Development Fund).

Acknowledgments

Not applicable**.**

Conflicts of Interest

The authors declare no conflicts of interest.

References

1. Luo T, Chao Z, Du S, Jiang L, Chen S, Zhang R, Han H, Han B, Wang Z, Chen, G, Mei Y. A Novel Multi-Scale Ceramic-Based Array (SiCb+B4Cp)/7075Al as Promising Materials for Armor Structure. *Materials* 2023; 16, 5796.
2. Yang R, Li K, Yin L, Ren K, Cheng Y, Li T, Fu J, Zhao T, Chen Z, Yang J. Study on the Penetration Power of ZrO2 Toughened Al2O3 Ceramic Composite Projectile into Ceramic Composite Armor. *Materials* 2022; 15, 2909.
3. Fejdyś M, Kośla K, Kucharska-Jastrząbek A, Łandwijt M. Influence of ceramic properties on the ballistic performance of the hybrid ceramic–multi-layered UHMWPE composite armour. *J. Aust. Ceram. Soc*. 2021; 57, 149–161.
4. Chen Z, Xu Y, Li M, Li B, Song W, Xiao L, Cheng Y, Jia S. Investigation on Residual Strength and Failure Mechanism of the Ceramic/UHMWPE Armors after Ballistic Tests. *Materials* 2022; 15, 901.
5. Cegła M. Special ceramics in multilayer ballistic protection systems. *Issues Armament Technol*. 2018; 147, 63–74.
6. Grujicic M, Pandurangan B, Zecevic U, Koudela K L, Cheeseman B A. Ballistic Performance of Alumina/S-2 glass reinforced polymer-matrix composite hybrid lightweight armor against armor piercing (AP) and non-AP projectiles. *Multidiscip. Model. Mater. Struct.* 2007; 3, 287–312.
7. Hogan J D, Farbaniec L, Mallick D, Domnich V, Kuwelkar K, Sano T, McCauley J W, Ramesh K T. Fragmentation of an advanced ceramic under ballistic impact: Mechanisms and microstructure. *Int. J. Impact Eng*. 2017; 102, 47–54.
8. Magier M. Methods of estimating the armor penetration depth by kinetic projectiles. *Issues Armament Technol*. 2007; 101, 103–115.
9. Ding L, Gu X, Shen P, Kong X. Ballistic Limit of UHMWPE Composite Armor under Impact of Ogive-Nose Projectile. *Polymers* 2022; 14, 4866.
10. Nair A N, Sundharesan S, Al Tubi M A A. Kevlar-based Composite Material and its Applications in Body Armour: A Short Literature Review. *IOP Conf. Ser.: Mater. Sci. Eng*. 2020; 987, 012003.
11. Kang T J, Kim C. Energy-Absorption Mechanisms in Kevlar Multiaxial Warp-Knit Fabric Composites Under Impact Loading. *Compos. Sci. Technol*. 2000; 60, 773–784.
12. Min S, Chen X, Chai Y, Lowe T. Effect of Reinforcement Continuity on the Ballistic Performance of Composites Reinforced with Multiply Plain Weave Fabric. *Compos. B Eng*. 2016; 90, 30–36.
13. Nurazzi N M, Asyraf M RM, Khalina A, Abdullah N, Aisyah H.A, Rafiqah S A, Sabaruddin F A, Kamarudin S H, Norrrahim M N F, Ilyas R A, Sapuan S M. A Review on Natural Fiber Reinforced Polymer Composite for Bullet Proof and Ballistic Applications. *Polymers* 2021; 13, 646.
14. Varma T V, Sarkat S. Designing polymer metamaterial for protective armor: a coarse-grained formulation. *Meccanica*. 2020; 56, 383-392.
15. Si P, Liu Y, Yan J, Bai F, Huang F. Ballistic Performance of Polyurea-Reinforced Ceramic/Metal Armor Subjected to Projectile Impact. *Materials* 2022; 15, 3918.
16. Colombo P, Zordan F, Medvedovski E. Ceramic–polymer composites for ballistic protection. *Adv. Appl. Ceram*. 2006; 105, 78-83.
17. Wiśniewski A B, Pacek D B, Żochowski P, Wierzbicki Ł, Kozłowska J, Zielińska D, Olszewska, K, Grabowska G, Błaszczyk

J, Pawłowska A, Wałęza J. Elastic armour, Patent no. PL224825 (B1), 2017.
18. Kośla K, Kubiak P, Fejdyś M, Olszewska K, Łandwijt M, Chmal-Fudali E. Preparation and Impact Resistance Properties of Hybrid Silicone-Ceramics Composites. *Appl. Sci*. 2020; 10, 9098.
19. Tang M, Huang G, Zhang H, Liu Y, Chang H, Song H, Xu D, Wang Z. Dependences of Rheological and Compression Mechanical Properties on Cellular Structures for Impact-Protective Materials. *ACS Omega* 2017, 2, 2214−2223.
20. Poron® XRDTM Extreme Impact protection – Physical Properties. https://www.algeos.com.au/pdfs/PORONXRDData Sheet.pdf [accessed on: 14.12.2023]
21. Venkatraman P D, Tyler D J, A critical review of impact resistant materials used in sportswear clothing. International conference in Advances in Textiles, Machinery, Nonwovens and Technical Textiles, ATNT, Coimbatore, India, 2011.
22. Bhagavathula K B, Azar A, Ouellet S, Satapathy S, Dennison C R, Hogan J D. High Rate Compressive Behaviour of a Dilatant Polymeric Foam. *J. Dyn. Behav. Mater*. 2018; 4, 573-585.
23. Zuckerman S L, Reynolds B B, Yengo-Kahn A M, Kuhn A W, Chadwell J T, Goodale S E, Lafferty C E, Langford K T, McKeithan L J, Kirby P, Solomon G S. A football helmet prototype that reduces linear and rotational acceleration with the addition of an outer shell. *J Neurosurg*. 2019; 130, 1634–1641.
24. Cushioning and impact absorbing foam. https://www.trelleborg.com/applied-technologies/products-and-solutions/advanced-energy-control-materials/confor-cushioning-and-impact-absorbing [accessed on: 15.12.2023]
25. Tsinas Z, Orski S V, Bentley V RC, Gonzalez Lopez L, Al-Sheikhly M, Forster A L. Effects of Thermal Aging on Molar Mass of Ultra-High Molar Mass Polyethylene Fibers. *Polymers* 2022; 14, 1324.
26. Yang X, Jia N. Hygrothermal effect on high-velocity impact resistance of woven composites. *Def. Technol*. 2022; 18, 823-833.
27. Liu Y, Wu Y. Influence of hydrothermal aging on the mechanical performance of foam core sandwich panels subjected to low-velocity impact. *Sci. Eng. Compos. Mater*. 2022; 29, 9–22.
28. Kośla K, Łandwijt M, Miklas M, Fejdyś M. Influence of the Accelerated Aging Process on the Fragment-Resistant Properties of Para-Aramid Body Armor. *Materials* 2022; 15, 6492.
29. Engelbrecht-Wiggans A, Burni F, Guigues E, Jiang S, Huynh T Q, Tsinas Z, Jacobs D, Forster A L. Effects of temperature and humidity on high-strength p-aramid fibers used in body armor. *Text. Res. J*. 2020; 90, 2428-2440.
30. Engelbrecht-Wiggans A, Tsinas Z, Krishnamurthy A, Forster A L. Effect of Aging on Unidirectional Composite Laminate Polyethylene for Body Armor. *Polymers* 2023; 15, 1347.
31. Fejdyś M, Kucharska-Jastrząbek A, Kośla K. Effect of Accelerated Ageing on the Ballistic Resistance of Hybrid Composite Armour with Advanced Ceramics and UHMWPE Fibers. *Fibres Text. East. Eur*. 2020; 28, 71-80.
32. Madej-Kiełbik L, Kośla K, Zielińska D, Chmal-Fudali E, Maciejewska M. Effect of Accelerated Ageing on the Mechanical and Structural Properties of the Material System Used in Protectors. *Polymers* 2019; 11, 1263.
33. Fejdyś M, Cichecka M, Łandwijt M, Struszczyk M.H. Prediction of the Durability of Composite Soft Ballistic Inserts. *Fibres Text. East. Eur*. 2014; 22, 81–89.
34. Brounstein Z, Zhao J, Geller D, Gupta N, Labouriau A. Long-Term Thermal Aging of Modified Sylgard 184 Formulations. *Polymers* 2021; 13, 3125.
35. Orn A. Degradation Studies on polydimethylsiloxane, Master thesis, Laboratory of organic chemistry, Faculty of Science and Engineering, Abo Akademi Univerity, Finland, 2019.
36. Dobrowolska E P. "Selection of the type and the proportion of chain extenders macromolecules polycarbonate-urethane from isophorone isocyanate" Master Thesis, Faculty of Materials Science and Engineering, Warsaw University of Technology, Warsaw, 2013.
37. Liu S H, Shen M Y, Kuan CF, Kuan H C, Ke C Y, Chiang C L. Improving Thermal Stability of Polyurethane through the Addition of Hyperbranched Polysiloxane. *Polymers* 2019; 11, 697.
38. Mikulčić H, Jin Q, Stančin H, Wang X, Li S, Tan H, Duić N. Thermogravimetric Analysis Investigation of Polyurethane Plastic Thermal Properties Under Different Atmospheric Conditions. *J. Sustain. Dev. Energy Water Environ. Syst.* 2019; 7, 355-367.
39. Petrie E M. Epoxy Adhesive Formulations, McGraw - Hill Professional, USA, 2006.
40. Szabelski J. Research on the influence of heat treatment of butt adhesive joints on their static strength. PhD Thesis, Faculty of Mechanical Engineering, Lublin University of Technology, Poland, 2014.
41. Rośkowicz M. The adhesive joint - the chosen problems of static service life. *Problemy Eksplotacji*, 2006; 3 , 91–105.